

# CompoNeRF: Text-guided Multi-object Compositional NeRF with Editable 3D Scene Layout

Haotian Bai<sup>1</sup> Yuanhuiyi Lyu<sup>1</sup> Lutao Jiang<sup>1</sup> Si Jia Li<sup>2</sup> Haonan Lu<sup>2</sup> Xiaodong Lin<sup>2</sup> Lin Wang<sup>1,3†</sup>

<sup>1</sup>VLIS LAB, AI Thrust, HKUST(GZ) <sup>2</sup>OPPO <sup>3</sup>Dept. of CSE, HKUST

haotianwhite@outlook.com, yuanhuiyilv@hkust-gz.edu.cn, jianglutao98@gmail.com,  
{lisijia, luhaonan, linxiaodong}@oppo.com, linwang@ust.hk

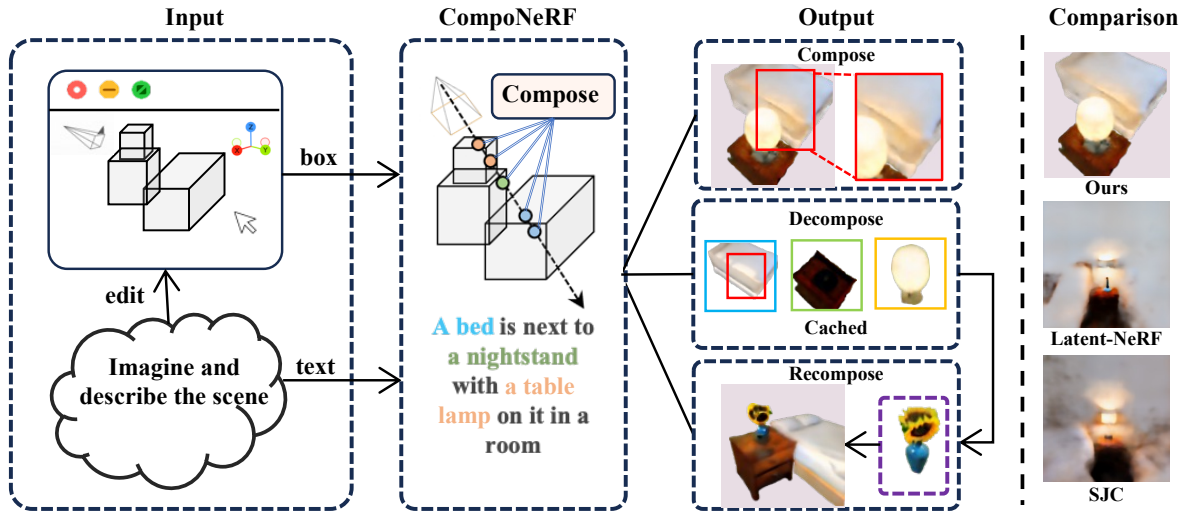


Figure 1. We introduce CompoNeRF, a novel framework that synthesizes coherent multi-object scenes by integrating textual descriptions with box-based spatial arrangements. CompoNeRF is designed for precision and adaptability, allowing for individual NeRFs, each denoted by a unique prompt color, to be composed, decomposed, and recomposed with ease, streamlining the construction of complex scenes from cached models after decomposition. The enhanced compositing effect of our method is accentuated by the red boxes, showcasing superior scene coherency compared to Latent-Latent-NeRF [22] and SJC [45].

## Abstract

Recent advances have shown promise in merging neural radiance fields (NeRFs) with pre-trained diffusion models for text-to-3D object generation. However, one enduring challenge is their inadequate capability to accurately parse and regenerate consistent **multi-object** environments. Specifically, these models encounter difficulties in accurately representing quantity and style prompted by multi-object texts, often resulting in a collapse of the rendering fidelity that fails to match the semantic intricacies. Moreover, amalgamating these elements into a coherent 3D scene is a substantial challenge, stemming from generic distribution inherent in diffusion models. To tackle the issue of ‘guidance collapse’ and enhance consistency, we pro-

pose a novel framework, dubbed **CompoNeRF**, by integrating an editable 3D scene layout with object specific and scene-wide guidance mechanisms. It initiates by interpreting a complex text into an editable 3D layout populated with multiple NeRFs, each paired with a corresponding subtext prompt for precise object depiction. Next, a tailored composition module seamlessly blends these NeRFs, promoting consistency, while the dual-level text guidance reduces ambiguity and boosts accuracy. Noticeably, the unique modularity of CompoNeRF permits NeRF decomposition. This enables flexible scene editing and recomposition into new scenes based on the edited layout or text prompts. Utilizing the open source Stable Diffusion model, CompoNeRF not only generates scenes with high fidelity but also paves the way for innovative multi-object composition using editable 3D layouts. Remarkably, our framework achieves up to a **54%** improvement in performance, as measured

† Corresponding author

by the multi-view CLIP score metric. Code is available at <https://github.com/hbai98/Componerf>.

## 1. Introduction

Recent advances in text-to-image generation have been driven by the integration of vision-language pre-trained models [16, 34] with state-of-the-art diffusion processes [9, 29, 36], leading to impressive outcomes. Pioneering text-to-3D approaches [8, 10, 11, 15, 26, 37, 50] have built upon these successes, employing these robust vision-language models to enrich 3D generative models with the structured understanding provided by Neural Radiance Fields (NeRFs) [4, 23, 28]. This synergy [17, 22, 32, 45] facilitates the creation of 3D models which, when rendered from different views, cohere with the learned text-to-image diffusion model distribution, opening new avenues for the direct synthesis of 3D content from textual descriptions.

Textual descriptions provide a broad specification for 2D images or 3D models, thus the translation into coherent visual representations, especially for scenes with multiple objects, is far from straightforward. Diffusion models, such as Stable Diffusion [36], have been extensively trained on vast text-image datasets [38], yet they often stumble when tasked with interpreting text involving multiple objects with sparse representation in the training data. This results in the generation of images that miss objects or depict them incorrectly. Fig. 2(a) exemplifies how Stable Diffusion does not reliably maintain the distinction and arrangement of objects in even simple multi-object scenarios. For instance, it might overlook an apple or banana or render them with inaccurate colors. This issue, known as ‘guidance collapse’, is particularly detrimental to the rendering of multi-object scenes with text prompts. As a consequence, sophisticated models like Latent-NeRF [22] and SJC [45] fall short in their ability to fully realize the complex arrangements described in multi-object texts, which severely constrains their use for composing 3D scenes from textual descriptions.

This provokes an intriguing question: *Can diffusion models, equipped with the generic distribution, not only discern and regenerate individual components as specified by a multi-object text but also integrate them into a consistent 3D scene?* Our initial tactic, as shown in Fig. 2(b.1), attempts to manage this by assigning each object to a distinct NeRF with a shared context, diverging from the traditional single-network scene encodings [17, 22, 32, 45]. This approach aims to improve object recognition, yet it’s prone to ‘guidance collapse’ due to the global text prompts’ inability to offer precise semantic delineation for individual objects. Inspired by more accurate rendering of single objects with targeted subtext prompts as seen in (a), the subsequent refinement in (b.2) utilizes specific textual supervision for each object. This tailored guidance con-

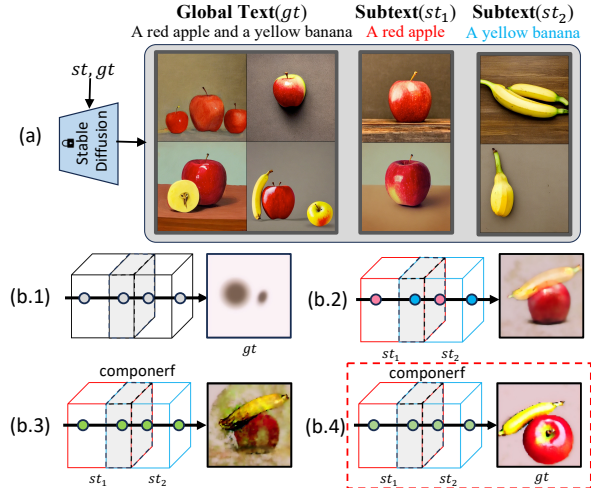


Figure 2. **The guidance collapse issue & Our solutions.** (a) Generation of multi-level scene utilizing the frozen Stable Diffusion. Instances of guidance collapse are observed when using global text ( $gt$ ). (b) Our proposed strategies for multi-object scene composition align with Eq. (2). The areas of NeRF overlap are indicated in gray. The green nodes represent composited samples. Our design is highlighted by the dashed box. 1. Apply  $gt$  as the overarching supervision. 2. Employ specific subtexts to direct each individual NeRF object. 3. Form composite samples by following step (2). 4. Refine the composite output with  $gt$ , building on step (3).

firms that diffusion models more effectively render individual objects when provided with explicit textual for each, thereby overcoming the ‘guidance collapse’ issue in complex multi-object scenarios. Nevertheless, the direct rendering of NeRFs often results in incorrect occlusions within their overlapping regions, indicating a deficiency in global refinement. To improve it, as detailed in (b.4), we refine sampling points that were originally guided by texts corresponding to individual objects, now with the incorporation of global textual guidance. This supplementary global oversight guarantees a harmonious rendering that upholds the unique identities of the objects while fostering overall compositional unity. Its vital role is underscored by its absence in (b.3), where its omission confirms its necessity.

We present **CompoNeRF**, a compositional NeRF framework that interprets multi-object text prompts as editable 3D scene layouts with granular text prompts, as shown in Fig. 1. The procedure begins by identifying individual objects from the textual description and positioning them within customizable 3D bounding boxes. Each box is supported by a distinct NeRF and a subtext label. Thus, CompoNeRF is designed to accommodate alterations, allowing for manipulations in the layout—like moving, scaling, or removal, as well as direct text edits. Our specialized composition module ensures that the global scene emerges not from a static assembly but from an orchestrated composi-

Methods	Diffusion Model	3D Representation	Scene Rendering	Input Prompt	Scene Editing	recomposition
DreamFusion	Imagen	Mip-NeRF 360 [5]	Object-centric	Text	T	✗
Magic3D	eDiff-I + SD	Instant-NGP [27]	Object-centric	Text	T	✗
DreamBooth3D	DreamBooth+DreamFusion	Mip-NeRF [3]	Object-centric	Text+Images	T	✗
Points-to-3D	ControlNet+Point-E	Instant-NGP	Object-centric	Text+Image	T	✗
Fantasia3D	SD+PBR	DMTET [39]	Object-centric	Text/Fine Shape	T/M/S/R	✓
Latent-NeRF	SD	Instant-NGP	Object-centric	Text+Fine Shape	T	✗
SJC	SD	voxel radiance field	Object-centric	Text	T	✗
<b>Ours</b>	SD	Instant-NGP	Object-compositional	Text+3D Layout	T/M/S/R	✓

Table 1. **Comparison of our method with the related works for text-to-image generation.** SD denotes Stable Diffusion. For scene editing, we use T(editing object with text), M(moving object), S(scaling object), and R(removing object) for short.

tion of these adaptable local models. The qualitative validation of CompoNeRF’s performance is presented in Table 1, benchmarking it favorably against contemporary methods.

CompoNeRF distinguishes itself with three core capabilities: it *composes* multi-object scenes from textual prompts, *decomposes* by archiving each NeRF for subsequent utilization, and *recomposes* by employing this curated content gallery to rapidly generate elaborate 3D scenes, thereby streamlining the workflow of 3D content creation.

Next, we introduce a more objective evaluation method to address the lack of rigorous quantitative analysis in prior works, which often rely solely on visual quality comparisons. By employing the averaged CLIP score [44] on rendering views of 3D content against global text prompts, we quantitatively measure the alignment of our generated scenes with their textual prompts, demonstrating the effectiveness of CompoNeRF in producing detailed and coherent 3D scenes that accurately reflect the given text descriptions.

To encapsulate, our paper makes three key contributions: **(I)** We address the ‘guidance collapse’ problem in creating multi-object 3D scenes. Our innovative use of editable 3D layouts coupled with multiple localized NeRFs allows for precise direction over individual object representations. Moreover, these localized NeRF models are designed to be storable and reusable, enhancing efficiency in scene composition. **(II)** We introduce a composition module enables fine-tuning of the rendering process and text-based guidance, ensuring both the distinctiveness of individual objects and the holistic integration within the scene. **(III)** We conduct extensive evaluations of CompoNeRF’s performance in multi-object scene generation, employing both qualitative and quantitative assessment for the multi-object text-to-3D task. The rigorous testing confirms that our CompoNeRF outperforms existing models in generating multi-object scenes that closely align with textual prompts.

## 2. Related Works

**Text-guided 3D Generative Models.** The integration of vision-language models like CLIP with 3D generative

methods has propelled text-guided 3D generation forward. Models that harness these advancements, such as those by Jain et al.[11] and Wang et al.[44], have excelled in aligning 3D renderings with text descriptors but often fall short in detail, limiting realism. Innovative approaches like DreamFusion [32], Magic3D [17], and Latent-NeRF [22] have sought to enhance this through text-to-image diffusion models and score distillation sampling in the latent space, with SJC [45] and DreamBooth3D [35] further refining the process to address distribution mismatches and enable image-based 3D generation, respectively. Points-to-3D [53] takes a novel route by utilizing 3D point clouds for guidance, whereas Fantasia3D [6] innovatively disentangles geometry and appearance tasks, it employs the Stable Diffusion model for learning geometry and utilizes the Physically-Based Rendering (PBR) material model [21] for appearance learning. Departing from these singular approaches, our CompoNeRF introduces a paradigm shift in the creation of intricate, multi-object 3D scenes. It adopts an *object-compositional* strategy, utilizing a novel editable 3D scene layout that conceptualizes the scene not as a singular, homogenous entity but as a constellation of discrete NeRFs. Each NeRF is meticulously associated with its spatial 3D bounding box and a corresponding descriptive text prompt, allowing for a dual-text guided compositional method together with the global text. This dual-text framework ensures that each object is not only individually delineated but also coherently integrated into the composite scene, thereby substantially elevating the authenticity of the generated 3D scenes. To ensure an equitable comparison, *we employ the same Instant-NGP backbone, Stable Diffusion checkpoint, and text prompts with Latent-NeRF and SJC.*

**Neural Rendering for 3D Modeling.** The evolution of NeRF has significantly elevated the capabilities of neural rendering. NeRF-based models [2, 4, 18, 19, 24, 28, 43] have redefined volume rendering [13] through the use of coordinate-based MLPs that infer color and density from spatial and directional inputs. Their capacity to produce photo-realistic views has cemented differential volume rendering as a key component in a variety of applications,

such as scene relighting [41, 54], dynamic scene reconstruction [7, 33, 42, 49], and scene and avatar editing [20, 52], as well as surface reconstruction [1, 12, 46]. Typically, these approaches rely on a *single* MLP to encode an entire scene, which may introduce ambiguity in differentiating between objects. Our method, in contrast, renders scenes through a composite of multiple NeRFs, each responsible for a distinct part of the scene. This compositional rendering takes into account the interrelations of NeRFs, enabling distinction of individual objects and their global consistency.

**Object-Compositional Scene Modeling.** The creation of new scenes from individual, object-centric components represents a significant trend in scene generation, as evidenced by existing research [25, 40, 48, 51, 52, 56]. These efforts typically adopt one of two approaches: semantic-based or 3D layout-based. Semantic-based methods enhance object representations by incorporating additional semantic information, such as segmentation labels [56], instance masks [48, 52], or features extracted using pre-trained vision-language models [25]. On the other hand, 3D layout-based approaches, exemplified by NSG [30] and its successors [40], focus on spatial coordinates, using explicit 3D object placement data to guide object and scene composition. Diverging from conventional techniques, our method innovates by utilizing decomposed, object-specific 3D layouts. This approach enables precise control over scene dynamics, encompassing both object-specific text prompt modifications [17, 32] and spatial manipulation. CompoNeRF’s distinctive feature lies in its capability to recompose scenes by interfacing with decomposed NeRFs, thereby accelerating the creation of new scenes, as highlighted in Table 1. In contrast to the mesh-based method in Fantasia3D, which requires considerable human effort in mesh modification and graphics engine support for editing, CompoNeRF offers a more streamlined process. Our composition module seamlessly integrates components, requiring only minimal adjustments in layout or text prompts, followed by fine-tuning of existing offline models to align with the global environmental context during training.

### 3. Method

To resolve the issue of guidance collapse, our principal strategy is to *decompose the scene into reusable components and compose/recompose them into a unified and consistent one*. This enables flexible control over the generated content with direct use of prompts and box layouts, as illustrated in Fig. 1. Our proposed CompoNeRF confers several key benefits: 1) **Semantic Coherence:** It reliably creates 3D objects with detailed textures and global consistency, exemplified by authentic light interactions, such as reflections on the bed surface. 2) **Modularity and Reusability:** CompoNeRF functions as an ensemble of independently trained NeRF models. These can be efficiently stored and

later retrieved from a cached dataset, enabling their reuse in various cases. 3) **Editability:** Our approach allows for flexible scene modification, such as interchanging the lamp for a vase filled with sunflowers or altering its scale, by simply adjusting the box dimensions for later finetuning. This feature enhances flexibility and creative possibilities.

#### 3.1. Preliminaries

Defining individual object bounding boxes as *local frames* and the overall scene coordinate system as the *global frame*, we build the foundation of NeRF and diffusion processes.

**3D Representation in Latent Space.** Our methodology capitalizes on the state-of-the-art text-to-image generative model—Stable Diffusion as described by Rombach et al[36]. We build upon the Latent-NeRF framework [22], which computes latent colors for individual objects by considering their sample positions within a localized frame. Specifically, it maps a three-dimensional point in local coordinates  $\mathbf{x}_l = (x_l, y_l, z_l)$  to a volumetric density  $\sigma_l$  and an associated color  $\mathbf{C}_l$ , expressed as  $(\mathbf{C}_l, \sigma_l) = f_{\theta_l}(\mathbf{x}_l, y_l, z_l)$ . Here,  $f$  represents a Multi-Layer Perceptron (MLP) characterized by parameters  $\theta_l$ . This NeRF-generated color is then assessed in the context of the Stable Diffusion model, using text prompts to guide NeRF toward spatially coherent inference with intricate context.

**Volume Rendering with Multiple Objects.** We extend the volume rendering process to accommodate multiple objects by assigning each a local frame, denoted as  $j$ , with NeRF parameters  $\theta_{l,j}$ . Drawing from the foundational NeRF approach [24], in each local frame, we integrate the color  $\mathbf{C}_l$  and density  $\sigma_l$  for points  $\mathbf{x}_l$  sampled along a ray  $\mathbf{r}_l$ , emanates from the camera origin  $\mathbf{o}_l$  in direction  $\mathbf{d}_l$ . This is formalized in the predicted color integration for  $\hat{\mathbf{C}}_l$  as:

$$\hat{\mathbf{C}}_l(\mathbf{r}_l) = \sum_{k=1}^N T_{l,k} (1 - \exp(-\sigma_{l,k} \delta_k)) \mathbf{C}_{l,k}, \quad (1)$$

where  $T_{l,k} = \exp\left(-\sum_{j=1}^{k-1} \sigma_{l,j} \delta_j\right)$  represents the transmittance to the  $k$ -th of total  $N$  sample, calculated exponentially over the cumulative density along  $\mathbf{r}_l$ , and  $\delta_k$  is the interval between adjacent samples. To synthesize a coherent scene, we transition from processing individual local frames to a collective global frame. Within this global context, we reconcile object attributes inferred from their individual local NeRFs for refined  $\sigma_g, \mathbf{C}_g$  along with  $T_{g,k}$ . The samples  $\mathbf{x}_g$  are ordered based on their spatial distances from the origin  $\mathbf{o}_g$  following the coordinate transformation. We then express the volumetric rendering of a ray  $\mathbf{r}_g$  integrating  $m$  objects within the global frame as follows:

$$\hat{\mathbf{C}}_g(\mathbf{r}_g) = \sum_{k=1}^{m*N} T_{g,k} (1 - \exp(-\sigma_{g,k} \delta_k)) \mathbf{C}_{g,k}. \quad (2)$$

**Score Distillation Sampling.** To facilitate the conversion from text descriptions to 3D models, DreamFusion [32]

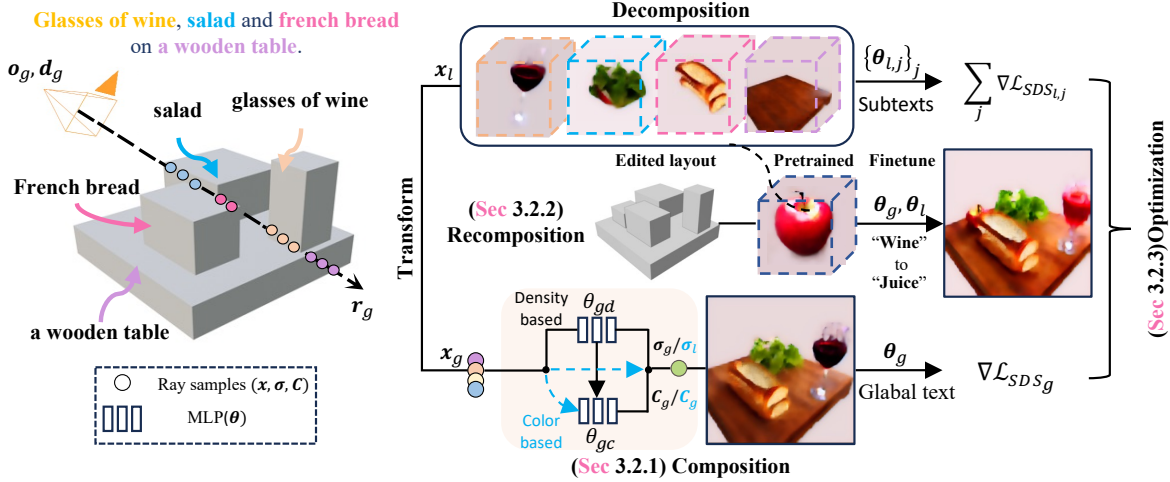


Figure 3. **Framework Overview.** The CompoNeRF model unfolds in three stages: 1) Editing 3D scene, which initiates the process by structuring the scene with 3D boxes and textual prompts; 2) Scene rendering, which encapsulates the composition/recomposition process, facilitating the transformation of NeRFs to a global frame, ensuring cohesive scene construction. Here, we specify design choices between density-based or color-based (without refining density) composition; 3) Joint Optimization, which leverages textual directives to amplify the rendering quality of both global and local views, while also integrating revised text prompts and NeRFs for refined scene depiction.

utilizes Score Distillation Sampling (SDS), leveraging the generative capabilities of a diffusion model, denoted as  $\phi$ , to guide the optimization of NeRF parameters, symbolized as  $\theta$ . Initially, SDS creates a noisy image  $X_t$  by infusing a randomly sampled noise  $\epsilon$ , which follows a normal distribution  $\mathcal{N}(0, I)$ , into a NeRF-rendered image  $X$  at a given noise level  $t$ . The diffusion model  $\phi$  then estimates the noise  $\epsilon_\phi(X_t, t, T)$  from this noisy image, conditioned by the noise level  $t$  and an optional text prompt  $T$ . The key step in SDS involves calculating the gradient of the loss function, which measures the discrepancy between the estimated noise and the originally added noise:

$$\nabla_{\theta} \mathcal{L}_{SDS}(X_t, T) = w(t) (\epsilon_\phi(X_t, t, T) - \epsilon), \quad (3)$$

where  $w(t)$  is a weighting function that adjusts the influence of the gradient based on the noise level. The gradients across all rendered views direct the update of  $\theta$ , ensuring that the NeRF-generated images align with the text descriptions. Additionally, we incorporate the 'perturb and average' technique from SJC for more robust  $\mathcal{L}_{SDS}$ . For a comprehensive understanding of these methods, the reader is directed to the detailed explanations provided in [32, 45].

## 3.2. The Proposed CompoNeRF

### 3.2.1 Composition Module

CompoNeRF is designed to composite multiple NeRFs to reconstruct scenes featuring multiple objects, utilizing guidance from both bounding boxes and textual prompts. Within our framework, depicted in Fig. 3, the Axis-Aligned Bounding Box (AABB) ray intersection test algorithm is applied to ascertain intersections across each box in the global frame.

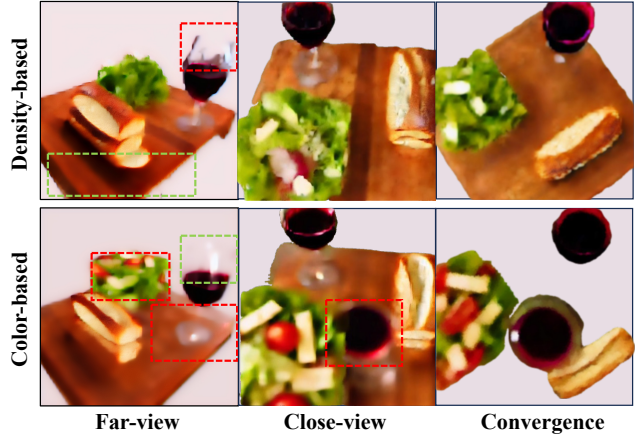


Figure 4. **Design Impact Comparison: Density vs. Color-based Methods.** The top row illustrates the density-based approach’s detailed rendering and quick convergence in the ‘table wine’ scene. The bottom row highlights the color-based method’s enhancements and its drawbacks, such as geometric and shadow inaccuracies, particularly in close-up views and slow convergence.

Subsequently, we sample points  $x_g$  within the intervals of the ray-box and project them to  $x_l$  to deduce the corresponding color  $C_l$  and density  $\sigma_l$  within individual NeRF models. These properties are processed through our composition module to infer the global color  $C_g$  and density  $\sigma_g$ , crucial for the global rendering. Volume rendering techniques [13] are then employed to procure the rendered views for both local and global frames. We propose dual SDS losses to ensure coherence between the image outputs

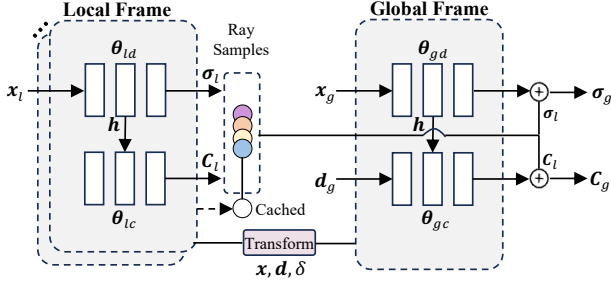


Figure 5. **Detail of Composition module:** density-based design.

and their corresponding textual descriptions. Additionally, our approach facilitates recomposition by channeling samples from cached models back into local frames along with the text revision, thereby streamlining the integration.

**Global Composition.** The independent optimization of each local frame may inadvertently result in a lack of global coherence within the scene. To address this, our scene composition process is designed to integrate these frames, thereby achieving a more consistent result. Before exploring the specifics of the module, it is imperative to discuss two critical design decisions within the composition module, as depicted in Fig. 3. Upon integrating the properties inferred from  $x_g$  into the composition module, they are fine-tuned through gradients derived from the global SDS loss. This process leads to a critical consideration: the necessity and implications of refining the global density  $\sigma_g$ . This can be divided into two approaches: **1) Density-based:** The advantage of adjusting  $\sigma_g$  is that it can adjust geometry, thus yielding a scene more congruent with the global text prompt. However, this comes at the cost of potentially compromising the optimal color  $C_g$ , as calibrating  $\sigma_g$  introduces more uncertainty for subsequent color refinement as it requires prior density features  $h$  as shown at Fig. 5. **2) Color-based:** Conversely, directly employing  $\sigma_l$  mitigates this uncertainty but at the expense of reduced geometric control, presenting a challenging balance to strike in the pursuit of precise scene composition. After thorough experiments, exemplified in Fig. 4, we have opted for the density-based approach to refine  $\sigma_g$  prioritizing both **accuracy and efficiency**. The test revealed that it excels in rendering intricate details, such as enhanced wood grain textures and more naturally contoured 'salad', as accentuated by boxes. This method also demonstrated a swifter convergence rate. Conversely, while the color-based improved reflections and reduced flickering on the 'wine cup', it was plagued by issues such as sparse density, which adversely brings holes at the base of the 'cup' and the corner of the 'table'. Furthermore, upon close examination, it becomes evident that shadow artifacts of 'wine' on the 'table' are pronounced, suggesting that its disadvantages outweigh its advantages.

**Network Design.** The compositional framework of our network, as delineated in Fig. 5, is predicated on an architecture that employs a suite of MLPs, represented as  $\{\theta_l\}_{l=1}^m$ , each dedicated to a distinct local frame. To harmonize  $\sigma_l$  and  $C_l$ , we incorporate global MLPs, including density calibrator  $f_{\theta_{gd}}$  and color calibrator  $f_{\theta_{gc}}$ . A transformation module complements this system, tasked with maintaining the spatial coherence between the global and local frames. It governs the transformation of sampling points  $x$ , ray directions  $d$ , and adjacent sampling distances  $\delta$ . This module also orders the points  $\{x_{g,j}\}_j$  by their distance to the global camera origin  $o_g$ , ensuring that each local point  $x_l$  is accurately matched with its corresponding global point  $x_g$  for subsequent volume rendering. The network design is:

$$\sigma_g = \alpha_d f_{\theta_{gd}}(x_g) + \sigma_l, \quad (4)$$

$$C_g = \alpha_c f_{\theta_{gc}}(h, d_g) + C_l. \quad (5)$$

In contrast to the local frames, the global frame's color output  $C_g$  is inferred based on  $h$  and conditional on  $d_g$  to enable a view-dependent lighting effect. Residual learning is leveraged here, where  $\sigma_l, C_l$  serve as foundational elements that support the learning of global density  $\sigma_g$  and color  $C_g$ . The parameters  $\alpha_d, \alpha_c$  are adjustable, allowing fine-tuning of the influence that local components exert on the global outputs. It is imperative to acknowledge that in our color-based method, density calibration is intentionally excluded to concentrate solely on the refinement of color dynamics as shown at Fig. 3. This is achieved by conditioning the process on both spatial and directional global inputs  $(x_g, d_g)$ , as demonstrated in the following equations:

$$\sigma_g = \sigma_l, \quad C_g = \alpha_c f_{\theta_{gc}}(x_g, d_g) + C_l. \quad (6)$$

The integration of extra  $x_g$  aims to facilitate a fair comparison under same inputs with the density-based. It enhances the visual appeal of effects like the wine cup's reflection, as demonstrated in Fig. 4. However, this method is not without its compromises. It tends to produce artifacts and is characterized by a slower convergence rate. Additionally, this approach limits the ability to precisely control density, subsequently impacting the intricate geometric details.

### 3.2.2 Recomposition

Our architecture advances scene reconstruction by providing an intuitive interface for layout manipulation. This capability is crucial for the reconfiguration of scene elements into novel scenes, as depicted in Fig. 3. Here, the input panel allows for adjustments in the attributes of bounding boxes, such as modifying the position and scale of the 'apple' bounding box prior to composition. The refinement process further involves sampling ray-box intervals from the global frame, leading to transformed coordinates with the corresponding ray samples that are then incorporated



Figure 6. **Qualitative comparison with other text-to-3D methods using multi-object text prompts.** Cases 1-3 demonstrate simpler settings characterized by compositions involving two objects. In contrast, Cases 4-8 delve into more intricate scenarios featuring compositions with more than two objects. Smaller images are presented to illustrate the generated local NeRFs (partially shown in Cases 4-8).

Method	Case 1	Case 2	Case 3	Case 4	Case 5	Case 6	Case 7	Case 8
LatentNeRF	25.16	27.07	27.69	31.19	21.55	26.32	27.43	29.51
SJC	23.55	27.84	28.21	30.53	23.33	27.41	25.62	28.76
<b>CompoNeRF (Ours)</b>	<b>26.13</b>	<b>32.71</b>	<b>33.37</b>	<b>31.45</b>	<b>36.06</b>	<b>28.44</b>	<b>28.96</b>	<b>30.98</b>

Table 2. **Performance comparison of our CompoNeRF in different 3D scenes.** For our evaluation metric, we utilize the average of CLIP scores [31, 47, 55] across different views, which serve to assess the similarity between the generated images and the global text prompt.

into the pipeline, as demonstrated in Fig. 5. Each bounding box represents an individual NeRF, providing the flexibility to move, scale, or remove elements as needed. CompoNeRF’s capabilities also extend to textual edits, exemplified by the transformation of ‘wine’ into ‘juice’. Since NeRFs have been well trained, we only finetune  $\theta_g, \theta_l$  to align text prompts to promote consistency of both local and global views. Moreover, the NeRFs once retrained within the edited scene, are also structured to be decomposable and cacheable in future scene compositions.

### 3.2.3 Optimization

During optimization, our method employs dual text guidance to align rendering results with both global and local textual descriptions. The optimization objective is:

$$\mathcal{L} = \alpha_g \nabla \mathcal{L}_{\text{SDS}}(\hat{\mathbf{X}}_g, T) + \alpha_l \sum_{j=1}^m \nabla \mathcal{L}_{\text{SDS}}(\hat{\mathbf{X}}_{l,j}, T_{l,j}) + \beta \mathcal{L}_{\text{sparse}},$$

where  $T$  signifies the global text prompt, while  $T_l$  pertains to a specific object within the global context. The hyperparameters  $\alpha_g, \alpha_l$ , and  $\beta$  modulate the respective loss weights. As suggested in [22], we use  $\mathcal{L}_{\text{sparse}}$  included to penalize the binary entropy of local NeRFs’ densities, thereby mitigat-

**Text:** *On the polished surface of the mahogany nightstand, a lamp with a shade of woven silk cast a warm glow over a Murano glass ball and its companion, a shimmering Dichroic glass ball, creating a dance of colors against the darkening twilight.*

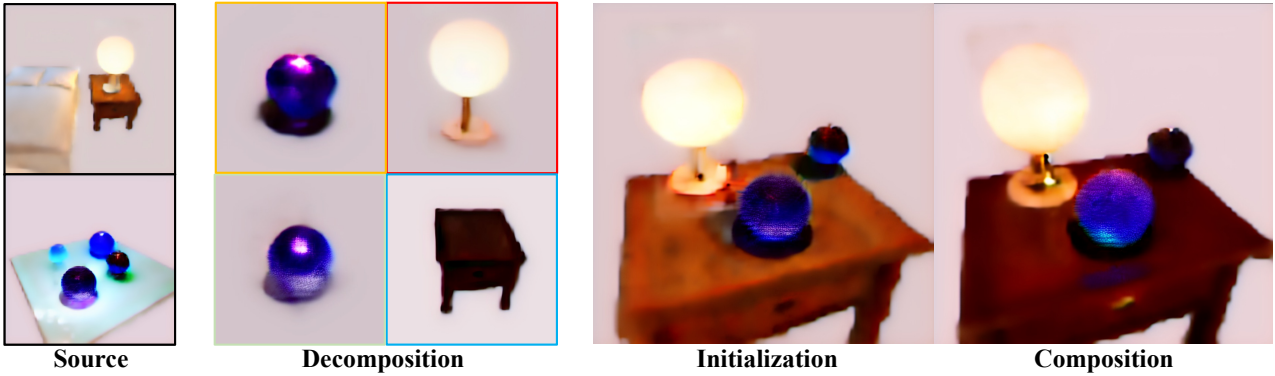


Figure 7. **Scene Editing Outcome:** Demonstrated here are the stages of our recombination, utilizing cached source scenes. Each NeRF is individually identified by colorful labels. These decomposed nodes are then positioned in the initial layout and subsequently calibrated to form the final composition. The detailed description of the ambient environment is underscored, enhancing the scene’s realism.

ing the issue of extraneous floating radiance. Additionally, incorporating directional cues such as “front view” or “side view” into the input text, as suggested by [22, 32] proves beneficial in specifying camera poses during the training phase, further enhancing the alignment of our generated scenes with the intended perspectives.

## 4. Experiments

### 4.1. Qualitative Comparison

In Fig. 6, we conduct qualitative comparisons of 3D assets generated using our method against Latent-NeRF and SJC, all based on the same Stable Diffusion model. Our method exhibits a remarkable ability to generate complex 3D models from a wide array of multi-object text prompts, demonstrating **superior object identity accuracy** and **enhanced context relevance and richness** compared to its counterparts. In simpler Case 3, our CompoNeRF method adeptly generates two distinct objects: a red *apple* and a yellow *banana*. In stark contrast, competing methods amalgamate the features of both fruits into a singular, indistinct object. Case 5, which is more intricate, showcases our method’s capability to render a realistic scene encompassing accurately depicted objects. Conversely, other methods struggle to produce even recognizable objects in this scenario. Note that we cannot corroborate the outcomes from DreamFusion [32] and Magic3D [17], as these models are predicated on closed-source diffusion models. Once these models are publicly available, integration with our CompoNeRF can further enhance their multi-object modeling capability.

### 4.2. Quantitative Comparison

In our study, we employ the CLIP score as the primary evaluation metric to assess the congruence between the gen-

erated 3D assets and the associated text prompts. This score, commonly used in text-to-image generation research as noted in studies [31, 47, 55], is derived from the cosine similarity between the embeddings of the text and the image, both encoded by the CLIP model. For 3D assets, we project images from various views and calculate the CLIP score concerning the global text prompt, with the overall CLIP score being the average of these values. As detailed in Tab. 2, our quantitative comparisons demonstrate the superior alignment of our method with the text prompt compared to the Latent-NeRF and SJC approaches in diverse scene configurations. Notably, in the challenging Case 5, our method shows a remarkable 54% improvement. The result of overall enhancement in multi-object scenes underscores the robustness of our global calibration strategy.

## 5. Discussion

Our proposed CompoNeRF represents a preliminary step in handling multi-object text for text-to-3D generation. It unleashes its potential by composing scenes with reusable NeRF components, which also facilitates later editing. Fig. 7 showcases our refined scene renderings originating from pre-trained source scenes. Our process commences with a foundational scene, to which we introduce additional entities, such as glass balls within a bedroom context. Each component of the scene is encapsulated by a localized NeRF. However, a direct amalgamation of these components can manifest various flaws—artifacts at the base of the lamp and incongruous shadows and reflections from the glass ball are notable, detracting from the authenticity of the scene’s ambiance. Subsequent to the manipulation phase, the reconfigured objects are adeptly integrated, achieving a coherent and consistent global scene in alignment with the edited layout. The nuanced changes in the



materials of the lamp, the nightstand, and their reflective surfaces demonstrates the system’s adaptability to diverse source inputs, which also involves a challenging text prompt containing subtle interplay within multi-object context.

**Limitations.** Our method has certain limitations: 1) restricted semantics processing, particularly interpreting uncommon object integration. 2) multi-face issue in the absence more intricate supervision. For more thorough evaluation, we direct readers to our *suppl.* materials.

## 6. Conclusion and Future Work

In this work, we have proposed a novel framework for multi-object text-guided compositional 3D scene generation with an editable 3D scene layout. Our framework interpreted a multi-object text prompt as a collection of localized NeRFs, each associated with a spatial box and an object-specific text prompt, which were then composited to render the entire scene view. We have further enhanced the framework with a specialized composition module for global consistency and dual-level text guidance, which effectively mitigated the issue of guidance collapse in the multi-object generation. Utilizing Stable Diffusion model, we have demonstrated that our method, the first to apply a compositional NeRF design to the text-to-3D task, can produce high quality 3D models that feature multiple objects and perform well compared with contemporaneous methods. Looking ahead, we have explored a promising application of CompoNeRF in the realm of scene editing, which allows for the reuse of trained models in scene recomposition. This capability opens up new possibilities and identifies a rich vein of future work to be pursued in this domain.

## References

- [1] Dejan Azinović, Ricardo Martin-Brualla, Dan B Goldman, Matthias Nießner, and Justus Thies. Neural rgb-d surface reconstruction. In *CVPR*, pages 6290–6301, 2022. 4
- [2] Haotian Bai, Yiqi Lin, Yize Chen, and Lin Wang. Dynamic plenotree for adaptive sampling refinement in explicit nerf. *ArXiv*, abs/2307.15333, 2023. 3
- [3] Jonathan T. Barron, Ben Mildenhall, Matthew Tancik, Peter Hedman, Ricardo Martin-Brualla, and Pratul P. Srinivasan. Mip-nerf: A multiscale representation for anti-aliasing neural radiance fields. *2021 IEEE/CVF International Conference on Computer Vision (ICCV)*, pages 5835–5844, 2021. 3
- [4] Jonathan T. Barron, Ben Mildenhall, Matthew Tancik, Peter Hedman, Ricardo Martin-Brualla, and Pratul P. Srinivasan. Mip-nerf: A multiscale representation for anti-aliasing neural radiance fields. In *ICCV*, pages 5835–5844. IEEE, 2021. 2, 3
- [5] Jonathan T. Barron, Ben Mildenhall, Dor Verbin, Pratul P. Srinivasan, and Peter Hedman. Mip-nerf 360: Unbounded anti-aliased neural radiance fields. *2022 IEEE/CVF Conference on Computer Vision and Pattern Recognition (CVPR)*, pages 5460–5469, 2021. 3
- [6] Rui Chen, Yongwei Chen, Ningxin Jiao, and Kui Jia. Fantasia3d: Disentangling geometry and appearance for high-quality text-to-3d content creation. In *Proceedings of the IEEE/CVF International Conference on Computer Vision (ICCV)*, 2023. 3
- [7] Chen Gao, Ayush Saraf, Johannes Kopf, and Jia-Bin Huang. Dynamic view synthesis from dynamic monocular video. In *ICCV*, pages 5712–5721, 2021. 4
- [8] Jun Gao, Tianchang Shen, Zian Wang, Wenzheng Chen, Kangxue Yin, Daiqing Li, Or Litany, Zan Gojcic, and Sanja Fidler. Get3d: A generative model of high quality 3d textured shapes learned from images. 2022. 2
- [9] Jonathan Ho, Ajay Jain, and Pieter Abbeel. Denoising diffusion probabilistic models. *Advances in Neural Information Processing Systems*, 33:6840–6851, 2020. 2
- [10] Fangzhou Hong, Mingyuan Zhang, Liang Pan, Zhongang Cai, Lei Yang, and Ziwei Liu. Avatarclip: Zero-shot text-driven generation and animation of 3d avatars. *arXiv preprint arXiv:2205.08535*, 2022. 2
- [11] Ajay Jain, Ben Mildenhall, Jonathan T Barron, Pieter Abbeel, and Ben Poole. Zero-shot text-guided object generation with dream fields. In *CVPR*, pages 867–876, 2022. 2, 3
- [12] Lutao Jiang, Ruyi Ji, and Libo Zhang. Sdf-3dgan: A 3d object generative method based on implicit signed distance function. *arXiv preprint arXiv:2303.06821*, 2023. 4
- [13] James T Kajiya and Brian P Von Herzen. Ray tracing volume densities. *ACM SIGGRAPH*, 18(3):165–174, 1984. 3, 5
- [14] Diederik P Kingma and Jimmy Ba. Adam: A method for stochastic optimization. *arXiv preprint arXiv:1412.6980*, 2014. 1
- [15] Han-Hung Lee and Angel X Chang. Understanding pure clip guidance for voxel grid nerf models. *arXiv preprint arXiv:2209.15172*, 2022. 2
- [16] Junnan Li, Dongxu Li, Caiming Xiong, and Steven Hoi. Blip: Bootstrapping language-image pre-training for unified vision-language understanding and generation. In *ICML*, pages 12888–12900. PMLR, 2022. 2
- [17] Chen-Hsuan Lin, Jun Gao, Luming Tang, Towaki Takikawa, Xiaohui Zeng, Xun Huang, Karsten Kreis, Sanja Fidler, Ming-Yu Liu, and Tsung-Yi Lin. Magic3d: High-resolution text-to-3d content creation. *arXiv preprint arXiv:2211.10440*, 2022. 2, 3, 4, 8
- [18] David B Lindell, Julien NP Martel, and Gordon Wetzstein. Autoint: Automatic integration for fast neural volume rendering. In *CVPR*, pages 14556–14565, 2021. 3
- [19] Lingjie Liu, Jiatao Gu, Kyaw Zaw Lin, Tat-Seng Chua, and Christian Theobalt. Neural sparse voxel fields. *ArXiv*, abs/2007.11571, 2020. 3
- [20] Lingjie Liu, Marc Habermann, Viktor Rudnev, Kripasindhu Sarkar, Jiatao Gu, and Christian Theobalt. Neural actor: Neural free-view synthesis of human actors with pose control. *ACM Transactions on Graphics (TOG)*, 40(6):1–16, 2021. 4
- [21] Stephen McAuley, Stephen Hill, Naty Hoffman, Yoshiharu Gotanda, Brian Smits, Brent Burley, and Adam Martinez. Practical physically-based shading in film and game production. In *ACM SIGGRAPH 2012 Courses*, 2012. 3
- [22] Gal Metzer, Elad Richardson, Or Patashnik, Raja Giryes, and Daniel Cohen-Or. Latent-nerf for shape-guided generation of 3d shapes and textures. *arXiv preprint arXiv:2211.07600*, 2022. 1, 2, 3, 4, 7, 8, 6
- [23] Ben Mildenhall, Pratul P. Srinivasan, Matthew Tancik, Jonathan T. Barron, Ravi Ramamoorthi, and Ren Ng. Nerf: Representing scenes as neural radiance fields for view synthesis. In *ECCV*, 2020. 2
- [24] Ben Mildenhall, Pratul P. Srinivasan, Matthew Tancik, Jonathan T. Barron, Ravi Ramamoorthi, and Ren Ng. Nerf: Representing scenes as neural radiance fields for view synthesis. In *ECCV*, pages 405–421. Springer, 2020. 3, 4
- [25] Ashkan Mirzaei, Yash Kant, Jonathan Kelly, and Igor Gilitschenski. Laterf: Label and text driven object radiance fields. In *Computer Vision–ECCV 2022: 17th European Conference, Tel Aviv, Israel, October 23–27, 2022, Proceedings, Part III*, pages 20–36. Springer, 2022. 4
- [26] Nasir Mohammad Khalid, Tianhao Xie, Eugene Belilovsky, and Tiberiu Popa. Clip-mesh: Generating textured meshes from text using pretrained image-text models. In *SIGGRAPH Asia 2022 Conference Papers*, pages 1–8, 2022. 2
- [27] Thomas Müller, Alex Evans, Christoph Schied, and Alexander Keller. Instant neural graphics primitives with a multiresolution hash encoding. *ACM Transactions on Graphics (TOG)*, 41:1 – 15, 2022. 3
- [28] Thomas Müller, Alex Evans, Christoph Schied, and Alexander Keller. Instant neural graphics primitives with a multiresolution hash encoding. *arXiv preprint arXiv:2201.05989*, 2022. 2, 3, 1
- [29] Alexander Quinn Nichol and Pratul P Dhariwal. Improved denoising diffusion probabilistic models. In *ICML*, pages 8162–8171. PMLR, 2021. 2

- [30] Julian Ost, Fahim Mannan, Nils Thuerey, Julian Knodt, and Felix Heide. Neural scene graphs for dynamic scenes. In *CVPR*, pages 2856–2865, 2021. 4
- [31] Gaurav Parmar, Krishna Kumar Singh, Richard Zhang, Yijun Li, Jingwan Lu, and Jun-Yan Zhu. Zero-shot image-to-image translation. In *ACM SIGGRAPH 2023 Conference Proceedings*, pages 1–11, 2023. 7, 8
- [32] Ben Poole, Ajay Jain, Jonathan T Barron, and Ben Mildenhall. Dreamfusion: Text-to-3d using 2d diffusion. *arXiv preprint arXiv:2209.14988*, 2022. 2, 3, 4, 5, 8
- [33] Albert Pumarola, Enric Corona, Gerard Pons-Moll, and Francesc Moreno-Noguer. D-nerf: Neural radiance fields for dynamic scenes. In *CVPR*, pages 10318–10327, 2021. 4
- [34] Alec Radford, Jong Wook Kim, Chris Hallacy, Aditya Ramesh, Gabriel Goh, Sandhini Agarwal, Girish Sastry, Amanda Askell, Pamela Mishkin, Jack Clark, et al. Learning transferable visual models from natural language supervision. In *ICML*, pages 8748–8763. PMLR, 2021. 2
- [35] Amit Raj, Srinivas Kaza, Ben Poole, Michael Niemeyer, Nataniel Ruiz, Ben Mildenhall, Shiran Zada, Kfir Aberman, Michael Rubinstein, Jonathan Barron, et al. Dreambooth3d: Subject-driven text-to-3d generation. *arXiv preprint arXiv:2303.13508*, 2023. 3
- [36] Robin Rombach, Andreas Blattmann, Dominik Lorenz, Patrick Esser, and Björn Ommer. High-resolution image synthesis with latent diffusion models. In *CVPR*, pages 10684–10695, 2022. 2, 4, 1
- [37] Aditya Sanghi, Hang Chu, Joseph G Lambourne, Ye Wang, Chin-Yi Cheng, Marco Fumero, and Kamal Rahimi Malekshah. Clip-forge: Towards zero-shot text-to-shape generation. In *CVPR*, pages 18603–18613, 2022. 2
- [38] Christoph Schuhmann, Romain Beaumont, Richard Vencu, Cade Gordon, Ross Wightman, Mehdi Cherti, Theo Coombes, Aarush Katta, Clayton Mullis, Mitchell Wortsman, et al. Laion-5b: An open large-scale dataset for training next generation image-text models. *arXiv preprint arXiv:2210.08402*, 2022. 2
- [39] Tianchang Shen, Jun Gao, K. Yin, Ming-Yu Liu, and Sanja Fidler. Deep marching tetrahedra: a hybrid representation for high-resolution 3d shape synthesis. In *Neural Information Processing Systems*, 2021. 3
- [40] Yeji Song, Chaerin Kong, Seoyoung Lee, Nojun Kwak, and Joonseok Lee. Towards efficient neural scene graphs by learning consistency fields. *arXiv preprint arXiv:2210.04127*, 2022. 4
- [41] Pratul P Srinivasan, Boyang Deng, Xiuming Zhang, Matthew Tancik, Ben Mildenhall, and Jonathan T Barron. Nerv: Neural reflectance and visibility fields for relighting and view synthesis. In *CVPR*, pages 7495–7504, 2021. 4
- [42] Edgar Tretschk, Ayush Tewari, Vladislav Golyanik, Michael Zollhöfer, Christoph Lassner, and Christian Theobalt. Non-rigid neural radiance fields: Reconstruction and novel view synthesis of a dynamic scene from monocular video. In *ICCV*, pages 12959–12970, 2021. 4
- [43] Dor Verbin, Peter Hedman, Ben Mildenhall, Todd E. Zickler, Jonathan T. Barron, and Pratul P. Srinivasan. Ref-nerf: Structured view-dependent appearance for neural radiance fields. In *CVPR*, pages 5481–5490. IEEE, 2022. 3
- [44] Can Wang, Menglei Chai, Mingming He, Dongdong Chen, and Jing Liao. Clip-nerf: Text-and-image driven manipulation of neural radiance fields. In *CVPR*, pages 3835–3844, 2022. 3
- [45] Haochen Wang, Xiaodan Du, Jiahao Li, Raymond A Yeh, and Greg Shakhnarovich. Score jacobian chaining: Lifting pretrained 2d diffusion models for 3d generation. *arXiv preprint arXiv:2212.00774*, 2022. 1, 2, 3, 5, 6
- [46] Peng Wang, Lingjie Liu, Yuan Liu, Christian Theobalt, Taku Komura, and Wenping Wang. Neus: Learning neural implicit surfaces by volume rendering for multi-view reconstruction. *Advances in Neural Information Processing Systems*, 34:27171–27183, 2021. 4
- [47] Su Wang, Chitwan Saharia, Ceslee Montgomery, Jordi Pont-Tuset, Shai Noy, Stefano Pellegrini, Yasumasa Onoe, Sarah Laszlo, David J Fleet, Radu Soricut, et al. Imagen editor and editbench: Advancing and evaluating text-guided image inpainting. In *Proceedings of the IEEE/CVF Conference on Computer Vision and Pattern Recognition*, pages 18359–18369, 2023. 7, 8
- [48] Qianyi Wu, Xian Liu, Yuedong Chen, Kejie Li, Chuanxia Zheng, Jianfei Cai, and Jianmin Zheng. Object-compositional neural implicit surfaces. In *Computer Vision—ECCV 2022: 17th European Conference, Tel Aviv, Israel, October 23–27, 2022, Proceedings, Part XXVII*, pages 197–213. Springer, 2022. 4
- [49] Wenqi Xian, Jia-Bin Huang, Johannes Kopf, and Changil Kim. Space-time neural irradiance fields for free-viewpoint video. In *CVPR*, pages 9421–9431, 2021. 4
- [50] Jiale Xu, Xintao Wang, Weihao Cheng, Yan-Pei Cao, Ying Shan, Xiaohu Qie, and Shenghua Gao. Dream3d: Zero-shot text-to-3d synthesis using 3d shape prior and text-to-image diffusion models. *arXiv preprint arXiv:2212.14704*, 2022. 2
- [51] Yinghao Xu, Menglei Chai, Zifan Shi, Sida Peng, Ivan Skorokhodov, Aliaksandr Siarohin, Ceyuan Yang, Yujun Shen, Hsin-Ying Lee, Bolei Zhou, et al. Discoscene: Spatially disentangled generative radiance fields for controllable 3d-aware scene synthesis. *arXiv preprint arXiv:2212.11984*, 2022. 4
- [52] Bangbang Yang, Yinda Zhang, Yinghao Xu, Yijin Li, Han Zhou, Hujun Bao, Guofeng Zhang, and Zhaopeng Cui. Learning object-compositional neural radiance field for editable scene rendering. In *ICCV*, pages 13779–13788, 2021. 4
- [53] Chaohui Yu, Qiang Zhou, Jingliang Li, Zhe Zhang, Zhibin Wang, and Fan Wang. Points-to-3d: Bridging the gap between sparse points and shape-controllable text-to-3d generation. *arXiv preprint arXiv:2307.13908*, 2023. 3
- [54] Xiuming Zhang, Pratul P Srinivasan, Boyang Deng, Paul Debevec, William T Freeman, and Jonathan T Barron. Nerfactor: Neural factorization of shape and reflectance under an unknown illumination. *ACM Transactions on Graphics (TOG)*, 40(6):1–18, 2021. 4
- [55] Zhixing Zhang, Ligong Han, Arnab Ghosh, Dimitris N Metaxas, and Jian Ren. Sine: Single image editing with text-to-image diffusion models. In *Proceedings of the IEEE/CVF Conference on Computer Vision and Pattern Recognition*, pages 6027–6037, 2023. 7, 8

- [56] Shuaifeng Zhi, Tristan Laidlow, Stefan Leutenegger, and Andrew J Davison. In-place scene labelling and understanding with implicit scene representation. In *ICCV*, pages 15838–15847, 2021. [4](#)

# CompoNeRF: Text-guided Multi-object Compositional NeRF with Editable 3D Scene Layout

## Supplementary Material

### 7. Supplementary Material

We provide more details of the proposed method and experimental results in the supplementary material. Sec.1 and Sec.2 provide the algorithm and more implementation details. Sec.3 provides more insights into our CompoNeRF model. Sec.4 adds more details of visualization results. Sec.5 lists our attached material details for both scene reconstruction and editing.

#### 8. 1. Algorithm

The detailed algorithm of training our proposed CompoNeRF is shown in Algorithm 1.

#### 9. 2. Implementation Details

For score distillation sampling, we use the v1-4 checkpoint of Stable Diffusion based on the latent diffusion model [36]. We utilize the code-base [22] for 3D representation and grid encoder from Instant-NGP [28] as our NeRF model. The global MLP consists 4 or 6 Linear layers with 64 hidden channels. In the training loss, we set  $\alpha_g = 100$ ,  $\alpha_l = 100$ , and  $\beta = 5e^{-4}$  if without specification. Our 3D scenes are optimized with a batch size of 1 using the Adam [14] optimizer on a single RTX3090. Our global frame is centered at the world origin and has a normalized side length of [-1,1]. To generate camera positions, we uniformly sample points on a hemisphere that covers the global frame with a random radius between 1.0 and 1.5. The camera distance can also be scaled in the way discussed in the main paper. Plus, cameras are oriented to look toward the objects. During optimization, the camera field of view is randomly sampled between 40 and 70 degrees. At test time, the field of view is fixed at 60 degrees. We use the Adam optimizer and perform gradient descent at a learning rate of 0.001 for 5,000 steps in simple prompts, such as “apple and banana”, and 8,000 steps in more complex prompts for better quality. We follow the implementation of SJC [45] to perform the averaging implicitly, relying on the optimizer’s momentum state when applying the perturb-and-average scoring strategy during training.

#### 10. 3. Discussion

##### More ablations on the design of composition module.

In Fig. 8, we present further results from the ablation study of our composition module. As outlined in our main manuscript, our preference for a density-based approach is

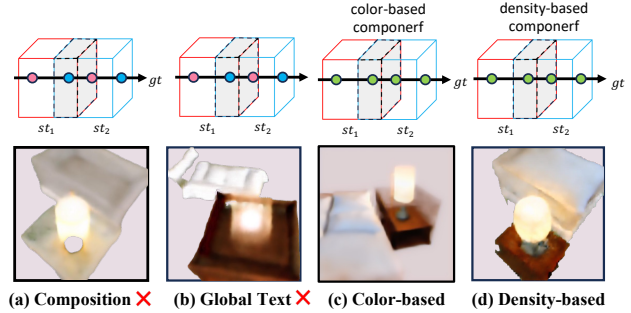


Figure 8. Ablation study on module designs with the scene bedroom. (a) without global calibration. (b) without global text loss. (c) color-based design. (d) our density-based design.

**Text:** *A bed is next to a nightstands where a table lamp on it in a room.*

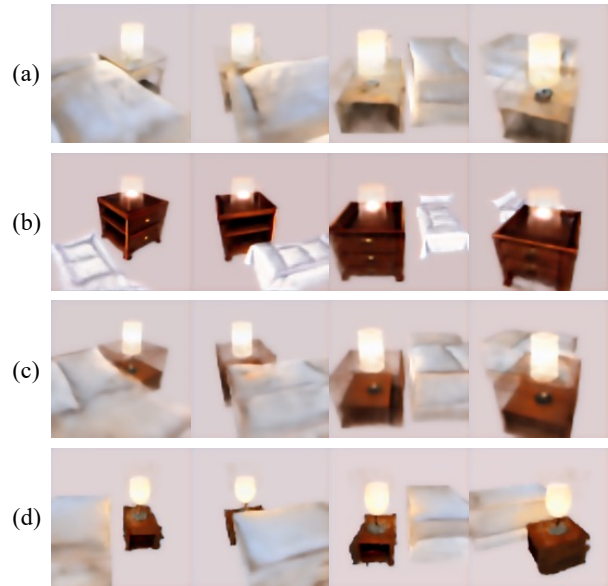


Figure 9. Multi view results with the text prompts on Fig. 8. Sub-texts for individual NeRFs are highlighted in bold.

due to its effective and precise calibration of global density. For example, the ‘bedroom’ scene builds upon the discussion from Fig.2(b.2) in the main paper. The complementary study in Fig. 8(a) demonstrates that direct global text supervision without compositional integration leads to a loss of material context, washing out the ‘bed’ and ‘nightstand’ in white. Conversely, Fig. 8(b) illustrates that omitting global

---

**Algorithm 1** Training for CompoNeRF

---

**Input:** a pre-trained text-to-image diffusion model  $\phi$ , multi-object text prompt  $T$  and a set of boxes for 3D scene layout.

**Output:** learned parameters of local NeRFs  $\{\theta_{l,i}\}_{i=1}^m$  and Global MLP  $\theta_g$ .

- 1: **for** Iter = 0 < MaxIter **do**
- 2:   Sample  $H \times W$  rays from the random camera position and add the directional prompt into  $T$ .
- 3:   **for**  $i = 0$  to  $H \times W$  **do**
- 4:     Calculate the ray-box intersection for ray  $r_i$  to get  $m_i$  hits.
- 5:     **for**  $j = 0$  to  $m_i$  **do**
- 6:       Sample  $N$  points with normalized location in the  $j$  hit local frame.
- 7:       Calculate color  $C_l$  and density  $\sigma_l$  for each point from  $\theta_{l,j}$ .
- 8:       Calculate the volumetric rendering color  $C_{l,i,j}$  of the local Frame for ray  $r_i$ .
- 9:     **end for**
- 10:   **end for**
- 11:   Map all points into global locations and sort them according to the depth.
- 12:   Calculate the calibrated color  $C_{g,i}$ ,  $\sigma_{g,i}$  via Eq. 4 and Eq. 5 for each point.
- 13:   Calculate the global volumetric rendering color  $C_{g,i}$  for each ray  $r_i$ .
- 14: **end for**
- 15: Generate the local view from  $\{C_{l,i,j}\}_{i=1}^{H \times W}$  and the global view from  $\{C_{g,i}\}_{i=1}^{H \times W}$
- 16: Perform score distillation sampling on the local render view and the global render view.
- 17: Update network parameters via an Adam optimizer.

**Eng:** Decompose local NeRFs and cache them into offline dataset.

---

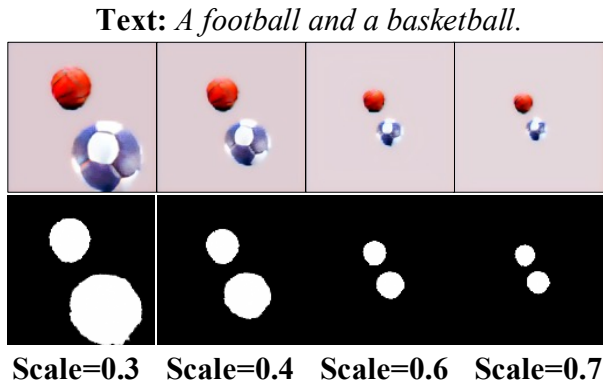


Figure 10. Results of using different training guidance resolutions by scaling the global frames. The first row is the rendering results, and the second row visualizes the rays that hit local frames.

text and relying solely on subtext supervision retains the familiar context of a ‘white sheet’ bed and a polished tan ‘nightstand’. However, this approach introduces geometric inconsistencies, such as an overly tall nightstand and a lamp lacking a base, along with an absence of light reflection in the surrounding space. The application of our composition module, depicted in Fig. 8(c) and 8(d), reveals that the density-based design affords enhanced control over density and, consequently, finer geometry. Instead of an empty space above the nightstand, the design aims to adjust the nightstand’s height to achieve scene harmony, although

it still exhibits limitations in controlling density, leading to subdued floating radiance. Fig. 9 provides a comprehensive visual comparison within the ‘bedroom’ context. When global calibration is absent, as seen in Fig. 9(a), the scene is plagued by sparse holes and a loss of color and texture detail. Neglecting the global branch entirely, as shown in Fig. 9(b), results in a lack of global consistency, evident in the disproportionate size of the ‘nightstand’ relative to the scene. Finally, the color-based solution in Fig. 9(c) fails to effectively correct the geometry, introducing additional artifacts. In contrast, the full model in Fig. 9(d) exhibits a marked improvement in these aspects.

#### **Optimizing Diffusion Model Guidance for Scene Resolution.**

A critical aspect of implementing our framework is the need to strike a balance between the overall scene’s resolution and the rendering details. For example, when a single object is placed within a vast scene, its rendered representation may be significantly reduced, occupying only a few pixels. This small pixel footprint can limit the amount of gradient information received during backpropagation. Fig. 10 illustrates this scenario using the same text prompt but with varying scales of the global frames, ranging from 0.3 to 0.7. The results underscore a key insight: the more pixel rays an object interacts with, the better the quality of its rendering. This finding is particularly relevant for large-scale scene rendering, where multiple local frames coexist within the same space. A small object in such a setup may receive minimal ray-box interactions, potentially leading to training inefficiencies or collapse. It’s also important to consider that our scene models are optimized in the la-

**Text:** *The game of black queen and white king chess was played on a table, with a glass of wine, and a table lamp providing the necessary illumination.*

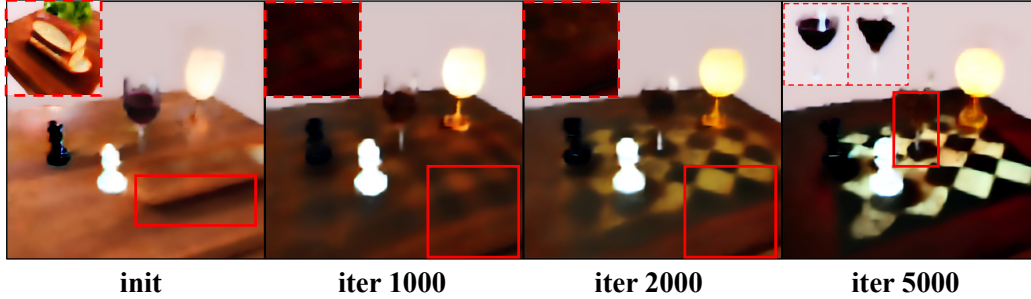


Figure 11. The ablation study on the scene recomposition, showcasing the finetuning process across different iteration steps and the resulting rendering views. Individual components are labeled in blue for clarity, while red boxes emphasize areas of contrast as discussed in the accompanying text.

tent space of the Stable Diffusion model, which has a feature resolution of  $64 \times 64$ . However, we decode these latent color features into RGB images with a resolution of  $128 \times 128$ . This discrepancy affects the density of rays throughout the space and, by extension, the number of objects that can be effectively rendered. Therefore, reconstructing large-scale scenes using our current model settings remains a challenging issue. As demonstrated in our papers, even small-scale scenes require approximately 5 hours of processing to learn from scratch, indicating potential limitations for larger-scale applications.

#### Influence of Global MLP Size on Composition Capabilities.

The complexity of a scene directly influences the required configuration of the parameters  $\theta_g$  within the composition module. In Figure 12, we experiment with varying the number of layers in the MLPs responsible for both densities  $f_{\theta_{g_d}}$  and color calibration  $f_{\theta_{g_c}}$ . The results indicate that an insufficiently representative MLP can fail to preserve the distinct identities of individual NeRFs. For instance, the 'white king chess' piece struggles to manifest its characteristic whiteness, leading the global calibrators to compensate inadequately by projecting a flattened representation onto the chessboard surface. By increasing the number of MLP layers, we observe a notable improvement in the accurate portrayal of each object's identity and overall scene quality. For example, the contextual details of the chessboard, like its grid pattern, are rendered more clearly and naturally. Based on these findings, we recommend fine-tuning this hyperparameter to align the composition module's capabilities with the specific complexity of the scene.

#### Global Context Assimilation by Local NeRFs and Composition Module.

As illustrated in Fig.1 of the main paper, our composition module integrates global context, accommodating comprehensive semantic details such as reflections on surfaces. Despite the primary embedding of context within the composition module, local NeRFs exhibit an ability to partially learn these global attributes. For

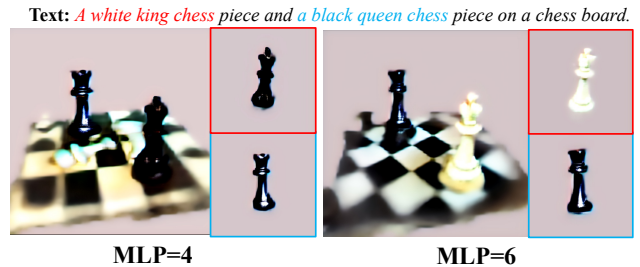


Figure 12. Ablation study on the learning capability of MLP. The selected scene components are accentuated by colorful boxes.

instance, Figure 11 shows that initially, the local NeRF optimization does not occur in isolation; the table, for example, bears a residual shadow from the 'french bread' in the original configuration as depicted at the upper left corner. As the training progresses, these anomalies are resolved, and the local NeRFs gradually assimilate aspects of the global texture, albeit to a limited extent. For instance, while the black and white pattern of the chessboard is predominantly captured by the global composition module, the local representation of the table, highlighted in red box in their upper left corners, remains unchanged. However, as iterations advance, despite there's no NeRF that is responsible for 'chess board', the global frame begins to discern it as the necessary environment and replicate the underlying 'chessboard' pattern. This reveals that NeRFs can initially embed global environmental context, while composition module can possibly merge some necessary local patterns for consistency.

#### Early Termination in the Scene Composition.

Our method's joint optimization aims to enhance the congruence between rendered views and multi-level text prompts. In later stages of training, the focus predominantly shifts to reinforcing global consistency as local fidelity typically reaches satisfactory levels by this point. The observations from the experiment depicted in Fig. 11 suggest a potential

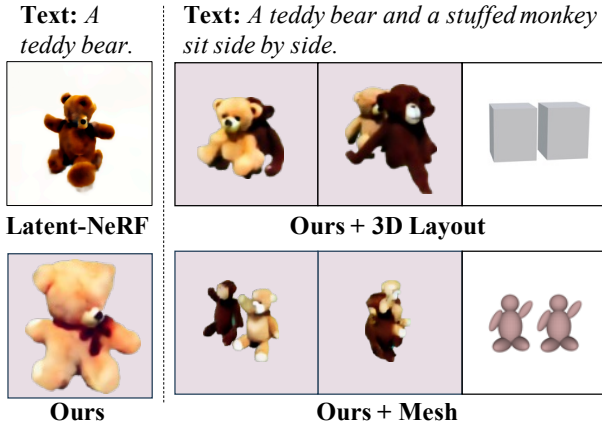


Figure 13. **(Left)** we observe the multi-face problem, *i.e.*, duplicated face views with geometry collapse in all methods, even in single-object cases. **(Right)** we provide mesh as guidance instead of box layouts to solve this problem, which further proves our method’s versatility and effectiveness.

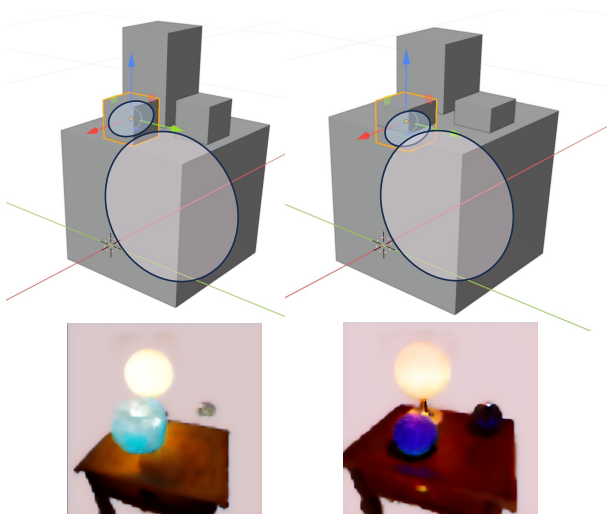


Figure 14. Ablation study examining layout editing and the challenge of floating objects. The upper row shows the layout editing and the lower row indicates rendering views. **(Left)** Renderings exhibit floating objects due to a suboptimal layout. **(Right)** Improved outcomes following layout refinements.

degradation in specific elements, such as the *wine*, which worsens as training progresses, as evidenced by the local frames’ comparison in the upper left corner. Concurrently, the global rendering depicts the *wine* as nearly imperceptible. This deterioration hints at the possibility that continued optimization may inadvertently diminish the representation of certain objects. Given these findings, we advocate for an early termination strategy when training models on less conventional scene compositions. This approach aims to

maintain an equilibrium between rendering fidelity and semantic coherence, preventing the over-attenuation of less common scene elements.

**Addressing Multi-face Issue with Enhanced Prompts.**

Much like Latent-NeRF and SJC, our CompoNeRF framework encounters the multi-face challenge, where guidance from the Stable Diffusion model may result in conflicting facial features for certain objects, as illustrated in Figure 13. The reason lies in the fact that diffusion model does not always provide reliable guidance that aligns with the desired orientation corresponding to the camera’s viewpoint during sampling. To mitigate the multi-face problem, stronger constraints can be introduced to promote geometric consistency within the 3D representation. CompoNeRF incorporates mesh constraints, akin to those utilized in Latent-NeRF, offering a more detailed 3D layout compared to traditional bounding boxes. As demonstrated in Figure 13, the implementation of exact mesh constraints markedly mitigates the multi-face issue, though it may come at the expense of detail and adaptability. Nevertheless, the requirement for accurate mesh input necessitates considerable manual editing, which may reduce the method’s range of applications. Despite this, our approach illustrates that the 3D scene layout can be readily adapted to accommodate a broader range of input prompts. Further study is needed to solve the persistent multi-face issue in the text-to-3D tasks.

**Layout Optimization to Address Floating Artifacts.**

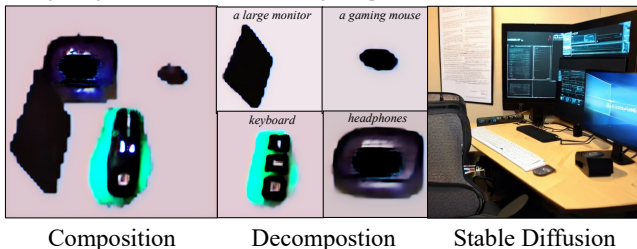
The process of scene composition begins with strategically positioning NeRFs within the predefined layout. An overlap of object bounding boxes is critical, as highlighted in Fig.2 of the main document, to facilitate the generation of convincing scenes. In our investigations, demonstrated in Fig. 14, we identified a ‘floating’ issue when bounding box overlaps are absent. This issue may stem from the regularization behavior within NeRFs, where the radiance fields—specifically, the regions responsive to gradient interactions, symbolized by ellipses centered on the boxes—fail to intersect. Such non-interaction can pose challenges, as it does not provide the necessary contiguous context for the global semantics to incorporate these objects seamlessly. To rectify this, one straightforward approach we recommend is the judicious repositioning of bounding boxes to introduce overlaps. For example, a slight downward adjustment of a box can instigate detectable overlaps during training, facilitating better integration. This insight opens up a potential avenue of research into the interplay between layout configurations and NeRFs, offering the possibility of more nuanced control over scene dynamics without the need for explicit layout modifications.

**Analysis of Failure Cases in Scene Composition and Editing.**

Our composition module may sometimes fail to produce coherent scenes, often due to limited text description distributions within the training data of diffusion mod-



**Text:** The computer station with a large monitor, a mechanical keyboard and gaming mouse, and noise-cancelling headphones.



**Text:** After a long day in space, the tired astronaut is standing by the bed.

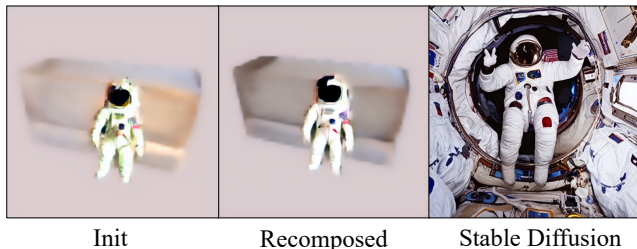
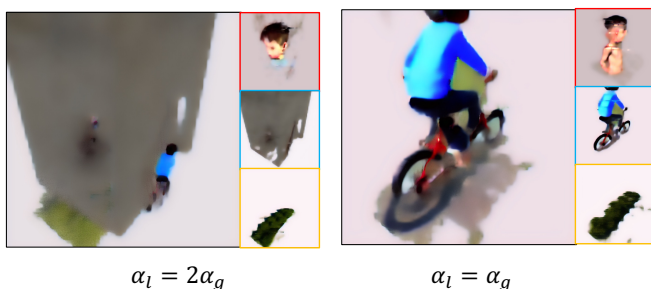


Figure 15. The failure cases are categorized as follows: **(Left)** issues encountered during scene reconstruction, and **(Right)** challenges arising in scene editing. The outputs from Stable Diffusion selected for illustration represent the most frequently occurring types generated by the model.

**Text:** The boy was gleefully riding his bike down the hill, feeling the wind rush past his face.



**Text:** The coffee sat next to a plate of warm croissants, creating a cozy breakfast scene on the rustic table.

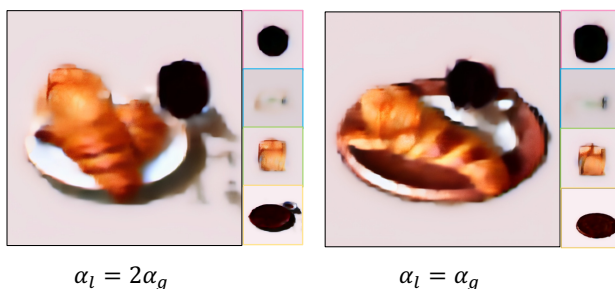


Figure 16. The failure cases with their color labeled NeRFs components shown beside. The textual guidance manipulation on global/local weights are shown below.

els as illustrated in Fig. 15. This can be mitigated by adjusting the loss weights governing the global and local guidance, such as Fig. 16. In scene composition, the ‘computer station’ lacks accessories like cables and wires, the ‘headphones’ are misshapen, and the ‘computer screen’ lacks a base. Scene reconstruction similarly shows the ‘astronaut’ and ‘bed’ placed together without sensible global calibration. Moreover, the Stable Diffusion model’s depiction of human figures often suffers from geometric distortions, potentially due to the multi-face problem, as shown in Fig. 16. These failures are mostly due to uncommon layouts or the rarity of certain objects in text-to-image datasets. Repeated global text prompts on Stable Diffusion and examination of numerous samples have failed to yield images that align with our objectives. This challenge extends beyond guidance collapse, reflecting the scarcity of certain objects in the model’s outputs. CompoNeRF’s effectiveness is inherently linked to the performance of large-scale text-to-image models, restricting its capabilities to generating primarily conventional scenes with well-defined global features. To address these limitations, we can strategically adjust the weights of global textual guidance  $\alpha_g \nabla \mathcal{L}_{SDS_g}$  and local textual guidance  $\alpha_l \nabla \mathcal{L}_{SDS_l}$ . This adjustment aims to find an equilibrium between the consistency of the overall scene

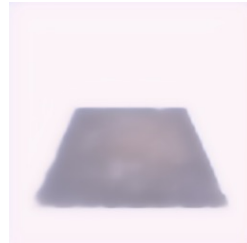
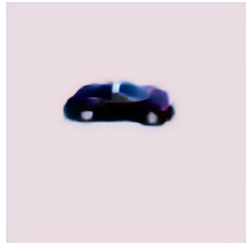
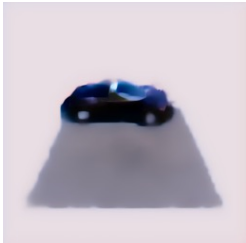
and the accuracy of individual components. For example, increasing  $\alpha_g$  enhances global consistency, as evidenced in Figure 16. However, this can inadvertently lead to objects assimilating extraneous global context. In the ‘boy riding bike’ scenario, a heightened  $\alpha_g$  may result in the ‘bike’ being erroneously represented as both a human figure and a bike. Similarly, in the ‘breakfast’ scene, amplifying global context might result in a more proportionate table, yet it complicates the distinction between the ‘croissant’ and its individual NeRF representation.

Ultimately, fine-tuning loss weight parameters is a delicate process that can mitigate identity issues, yet it demands careful calibration to maintain a harmony between scene integrity and the authenticity of each component. The limited representation of certain objects in pre-trained models remains a substantial obstacle, underscoring the need for further investigation into the issue of inadequate guidance in complex scene generation.

## 11. 4. More Visualization Results

We provide the multi-view qualitative results from CompoNeRF in Fig. 17. Note that we increase the resolution of the image latent features from  $64 \times 64$  to  $128 \times 128$  dur-

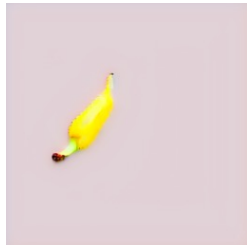
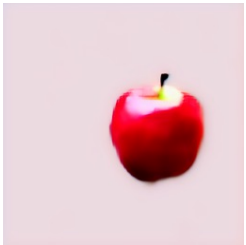
ing inference for better results. We also have attached video results in the supplemental materials for each case and the baseline Latent-NeRF [22] and SJC [45]. We have named each file after the text prompt used to generate the 3D asset. Please see the attached videos.



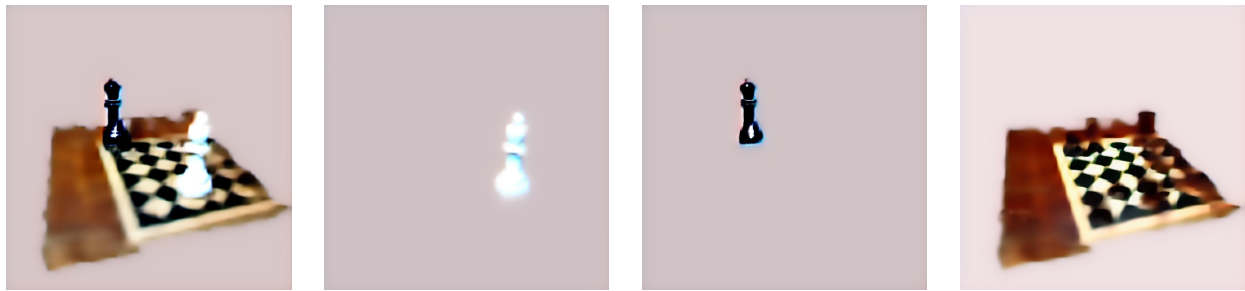
A tesla model three is running on the road.



An astronaut is standing on the moon ground.



A red apple and a yellow banana.



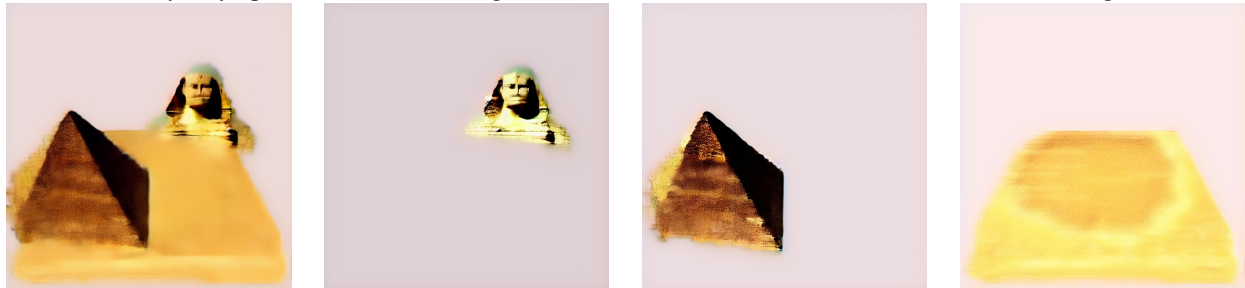
A white king and a black queen chess piece on a chess board.



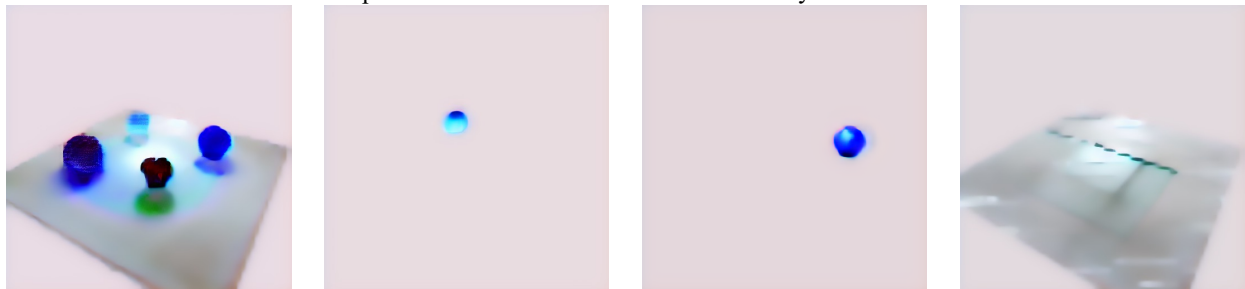
Glasses of wine, salad and french bread on a wooden table.



The Sydney Opera House, the Leaning Tower of Pisa, and the Eiffel Tower are situated in a triangle.



The Great Sphinx of Giza is situated near the Great Pyramid in the desert.



Crystal ball, Dichroic glass ball, Murano glass ball, and Solar-powered glass ball are placed on the glass table.

Figure 17. More qualitative results using multi-object text prompts.

## 12. Material Details

Denote recomposition results from the source scenes with xxx.mp4 consisting of Y) 'xxx', where Y is the source scene sign. The video attached to our supplementary materials consists of the following sections:

1. Qualitative Comparison Video:
  - (a) (tesla.mp4) A tesla model three is running on the road.
  - (b) (astronaut.mp4) An astronaut is standing on the moon ground.
  - (c) (apple\_banana.mp4) A red apple and a yellow banana.
  - (d) (chess.mp4) A white king and a black queen chess piece on a chess board.
  - (e) (table\_wine.mp4) Glasses of wine, salad and french bread on a wooden table.
  - (f) (pisa\_eiffel\_opera.mp4) The sydney opera house, the Leaning tower of Pisa, and the Eiffel tower are situated in a triangle.
  - (g) (sphinx.mp4) The Great Sphinx of Giza is situated near the Great Pyramid in the desert.
  - (h) (glass\_ball.mp4) Crystal ball, Dichroic glass ball, Murano glass ball, and Solar-powered glass ball are placed on the glass table.
  - (i) (bed\_room.mp4) A bed is next to a nightstand with a table lamp on it in a room.
  - (j) (vase\_flower.mp4) A bunch of sunflowers in a bar-nacle encrusted clay vase.
2. Scene Editing Video:
  - (a) (table\_chess.mp4) consists of d)'white king chess', e)'glass of whine', d)'black queen chess', i)'a table lamp', and e)'a table'.
  - (b) (table\_juice.mp4) consists of 'Glasses of juice', c)'apple', e)'french bread', e)'wooden table'.
  - (c) (table\_chess\_only.mp4) consists of d)'white king chess', d)'black queen chess', i)'a table lamp', and e)'a table'.
  - (d) (table\_balls.mp4) consists of h)'Murano glass ball', h)'Dichroic glass ball', i)'a table lamp', and e)'a table'.
3. Ablation Study Video:
  - (a) (bed\_room\_without\_calibration.mp4) deprived of calibration module for *bed room*.
  - (b) (bed\_room\_without\_global\_text.mp4) deprived of global branch/global text guidance for *bed room*.
  - (c) (bed\_room\_color\_based.mp4) color-based calibration module for *bed room*.
  - (d) (bed\_room\_full.mp4) our density-based calibration module for *bed room*.
  - (e) (table\_wine\_color\_based.mp4) color-based calibration module for *table wine*.
  - (f) (table\_wine\_density\_based.mp4) density-based cal-

ibration module for *table wine*.

### Training and Validation Demo

The demonstration of the training and validation process of the 'table\_wine' scene is incorporated in a specialized subfolder titled *example*.

### Training Process File Naming

Files in the training process adhere to a specific naming convention:

- **Format:** step-{num}-{local/global}-{id}\_image
  - num: Training step number.
  - local/global: Indicates local or global frames in the training model.
  - id: NeRF node index.

Files ending with *weights\_sum* denote the ray hit that receives gradients, integral in image processing or neural rendering.

### Validation Stage

The validation stage involves:

- A circular camera trajectory for comprehensive model assessment.
- Attachment of inferred surface norms, following the training process's naming convention.